Heat capacity, lattice dynamics, and thermodynamic stability of the negative thermal expansion material $HfMo_2O_8$

Catherine A. Kennedy and Mary Anne White*
Department of Chemistry and Institute for Research in Materials, Dalhousie University, Halifax, Nova Scotia B3H 4J3, Canada

Angus P. Wilkinson
School of Chemistry and Biochemistry, Georgia Institute of Technology, Atlanta, Georgia 30332-0400, USA

Tamas Varga
Thermochemistry Facility and NEAT ORU, University of California at Davis, Davis, California 95616, USA
(Received 9 January 2007; published 11 June 2007)

We explore the lattice dynamics of the negative thermal expansion material, cubic $HfMo_2O_8$, through analysis of its heat capacity (measured from 0.5 to 300 K) and its room-temperature Raman spectrum. Its heat capacity is quantitatively very similar to that of ZrW_2O_8, as is its Raman spectrum. The heat capacity of $HfMo_2O_8$ can be well represented by the present lattice dynamical assignment and by $C_P(HfW_2O_8) - C_P(ZrW_2O_8) + C_P(ZrMo_2O_8)$, but not by $C_P(HfO_2) + 2C_P(MoO_3)$, likely because the AB_2O_8 compounds have low-frequency optic modes, not present in HfO_2 and MoO_3. The present thermodynamic data also allow an analysis of the thermodynamic stability of cubic $HfMo_2O_8$, and it is shown to be unstable with respect to MoO_3 and HfO_2 at room temperature.

DOI: 10.1103/PhysRevB.75.224302 PACS number(s): 63.20.−e, 65.40.Ba, 65.40.−b, 82.60.Fa

I. INTRODUCTION

Framework solids of the general formula AB_2O_8 can exhibit negative thermal expansion (NTE) over a wide temperature range—for example, from 0.5 to 1050 K for ZrW_2O_8.[1–3] Other members of this family include $ZrMo_2O_8$ and $HfMo_2O_8$ and solid solutions such as $Zr_{1-x}Hf_xMo_{2-y}W_yO_8$ $(0 \leqslant x \leqslant 1,\ 0 \leqslant y \leqslant 2)$.[4] Many of these compounds exhibit polymorphism. The focus of the present work is on the cubic polymorph of hafnium molybdate $HfMo_2O_8$ (space group $Pa\bar{3}$, with $Z=4$). This phase is isostructural with β-ZrW_2O_8 but will be referred to here as cubic-$HfMo_2O_8$ or simply $HfMo_2O_8$ although it is distinct from the monoclinic polymorph β-$HfMo_2O_8$.[5] $HfMo_2O_8$ does not exhibit the cubic-to-cubic phase transition observed in ZrW_2O_8, as the former adopts the high-temperature disordered phase at all temperatures.[4] As for α- and β-ZrW_2O_8, $HfMo_2O_8$ is metastable under ambient conditions with respect to the simple oxides,[5] although it can be prepared through a nonconventional low-temperature synthesis.[4,6] Cubic-$HfMo_2O_8$ exhibits NTE: $\alpha_l = -4.0 \times 10^{-6}$ K^{-1} as determined from powder x-ray diffraction over the temperature range $T=77-573$ K.[4] At ambient temperature and pressures, the stable form of $HfMo_2O_8$ is trigonal.[7] Under high-pressure and high-temperature conditions, a monoclinic polymorph is obtained.[8,9] There has been prior interest in the thermodynamic properties[10–12] and vaporization behavior[13] of $HfMo_2O_8$ since hafnium and zirconium molybdate are major fission products in nuclear reactors.

II. EXPERIMENTAL METHODS

$HfMo_2O_7(OH)_2 \cdot 2H_2O$ was produced by the reaction of aqueous solutions of $HfCl_2O \cdot 8H_2O$ (Alfa Aesar, Ward Hill, MA) and $(NH_4)_6Mo_7O_{24} \cdot 4H_2O$ (Strem Chemicals, Newburyport, MA) in acid medium during 3 days of refluxing. Then $HfMo_2O_7(OH)_2 \cdot 2H_2O$ was dehydrated by a series of low-temperature heat treatment steps (350 °C for 12 h, 375 °C for 20 min, 400 °C for 20 min, 425 °C for 30 min, 450 °C for 30 min, 475 °C for 30 min, and finally an additional 30 min at 475 °C).

Thermogravimetric analysis gave a Hf:Mo mole ratio of 1:2.03. From x-ray diffraction, the content of trigonal $HfMo_2O_8$ was estimated to be ~0.1%. Differential scanning calorimetry from $T=300$ K to 460 K indicated no thermal anomalies and put an upper limit on water content of 0.5 mass%. To check the sample's amorphous content, laboratory powder x-ray diffraction data were collected on 70:30, 60:40, and 50:50 mass percent mixtures of $HfMo_2O_8$ with an internal standard Y_2O_3. The data were analyzed using the Rietveld method to obtain mass fractions for the two major crystalline phases. The sample was estimated to be 92% crystalline cubic $HfMo_2O_8$ from these mass fraction determinations. The remaining 8 ± 1 mass% impurities could include other phases of $HfMo_2O_8$ (e.g., trigonal or amorphous).

The sample was kept under vacuum except when making pellets for thermal measurements, when it was exposed briefly to air. The $HfMo_2O_8$ powder was pressed into disk-shaped pellets with a diameter of 4.74 mm using a load of 2000 lbs (0.5 GPa). We were concerned about the effect of pressure on the sample since high-pressure x-ray diffraction studies have shown that cubic-$HfMo_2O_8$ undergoes a fully reversible first-order phase transition between 0.7 and 2.0 GPa,[8] and under nonhydrostatic conditions cubic-$HfMo_2O_8$ starts to amorphize above 0.3 GPa.[8] However, x-ray diffraction carried out before and after pressing of the pellets showed no evidence of peak broadening and no new peaks in the diffraction pattern, indicating that pressing did not change the sample.

The Raman spectra for $HfMo_2O_8$ were obtained at room temperature on a Bruker RFS 100 spectrometer using the

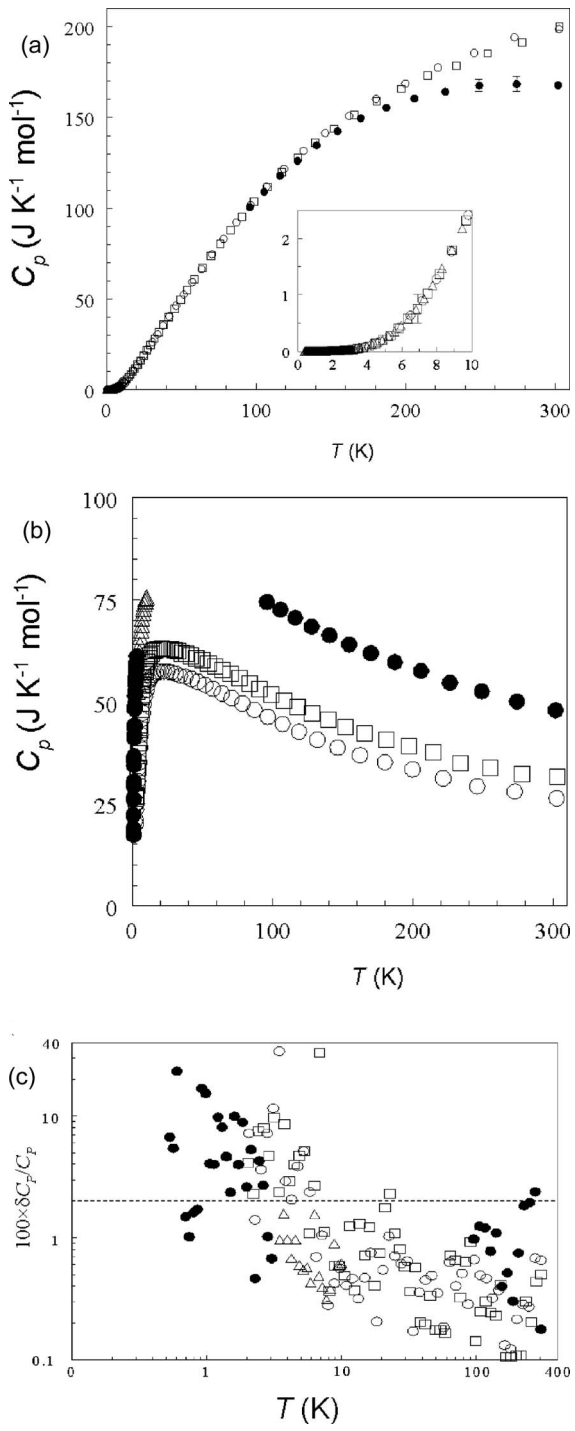

FIG. 1. Hafnium molybdate: (a) heat capacities, (b) relative sample contributions to the total heat capacities, and (c) estimated uncertainty. PPMS relaxation calorimeter, ^{4}He system: ○ 10.781±0.010 mg, □ 14.002±0.010 mg. ^{3}He system: △ 10.230±0.010 mg, ● 25.804±0.005 mg. Error bars are not visible where the symbol size is larger than the calculated uncertainty. The dotted line in (c) represents 2%.

1064.5-nm line of a Nd:YAG laser with an incident power of 147 mW. The scattered light was collected using a Ge diode detector. The samples were prepared by packing a small amount of the powder into a small hole located in the middle

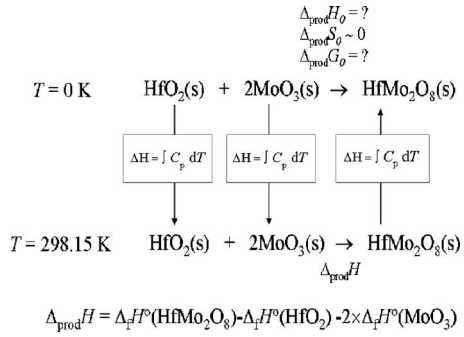

FIG. 2. Thermodynamic cycle to study the production of $HfMo_2O_8$ from HfO_2 and MoO_3.

of circular metal disks. The spectra were taken using 6000 scans at a resolution of 2 cm^{-1}.

The heat capacity of $HfMo_2O_8$ was measured for T=0.4–300 K using a commercial relaxation calorimeter (PPMS, physical property measurement system from Quantum Design). The heat capacity is determined by modeling the thermal relaxation response of the sample after heating, based on methods of Hwang *et al.*[14]

The pressed pellets were broken into pieces to obtain suitable samples for calorimetry. Samples of masses 10.781±0.010 mg and 14.002±0.010 mg were measured with the ^{4}He system and 10.230±0.010 mg and 25.804±0.005 mg with the ^{3}He system. We recently have shown that it is important to measure several samples of different masses with the PPMS relaxation calorimeter, in order to obtain accurate results.[15]

III. RESULTS AND DISCUSSION

A. Heat capacity of $HfMo_2O_8$

The experimental heat capacities of $HfMo_2O_8$ measured using the PPMS are shown in Fig. 1, along with the estimated uncertainties, and the relative contribution of the sample to the total heat capacity. The estimated uncertainties were calculated using standard propagation of errors and were based on the greater value of either the error calculated by twice the χ^2 statistics directly from the PPMS data or the standard propagation of error based on the standard deviation of the sample mass, the addenda heat capacity measurement, and the total heat capacity measurement. No phase transitions were observed over the temperature range 0.5 K$<T<$305 K.

Due care must be taken to achieve high accuracy in the heat capacity measurements to understand lattice dynamics: early heat capacity measurements of ZrW_2O_8 (Ref. 16) did not agree with later measurements.[17–19] Figure 1(a) shows that there are deviations among the heat capacity determinations of samples of $HfMo_2O_8$ of varying masses and especially that the largest sample size used, ~25 mg, deviates greatly from the other data for $T>150$ K. Neither the sample coupling nor the temperature fits seem to be responsible for this deviation; most likely, it is due to the low thermal conductivity of this material,[20,21] as for ZrW_2O_8.[15,22] Therefore the data for the ~25 mg sample for $T>150$ K are consid-

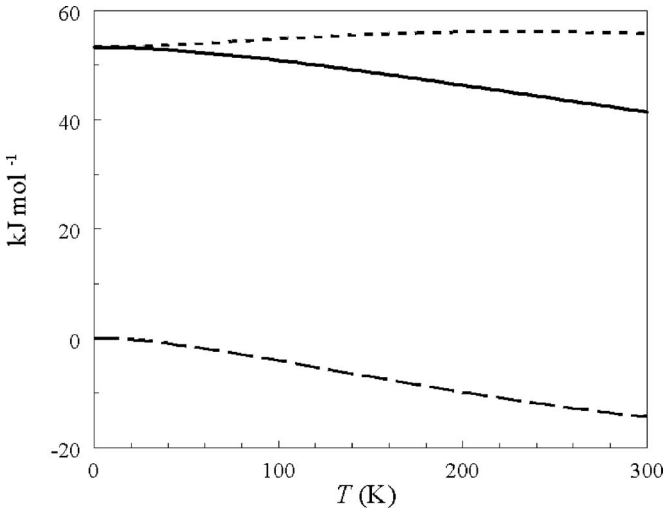

FIG. 3. The values of $\Delta_{prod}G$ (solid line), $\Delta_{prod}H$ (short-dashed line), and $-T\times\Delta_{prod}S$ (long-dashed line), for production of $HfMo_2O_8$(s) from HfO_2(s) and MoO_3(s), as functions of temperature.

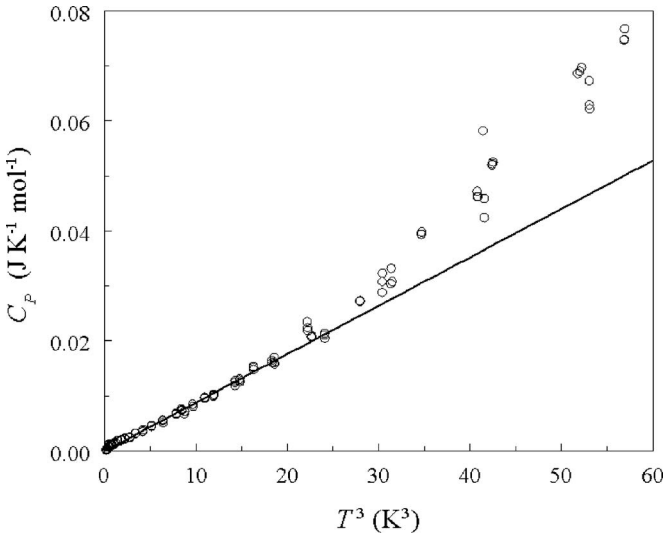

FIG. 4. C_P vs T^3 of $HfMo_2O_8$ for $T<4$ K. The solid line shows the Debye-T^3 law fit below $T=2.6$ K.

ered inaccurate and are not included in the subsequent discussion. Furthermore, the calculated heat capacity uncertainties [Fig. 1(c)] become large when the relative sample contribution to the total heat capacity [Fig. 1(b)] is small at low temperatures. Data with large fit deviations, as determined by the mean-squared deviation of the fit from the model expressed as a normalized χ^2 (Ref. 23) or with poor thermal contact as discerned from the sample coupling parameter[15] as assessed by the PPMS software, are not included in the subsequent analysis. The effect of the impurity content on heat capacity accuracy would be worst if the impurity were entirely amorphous $HfMo_2O_8$; this would lead to reported heat capacities ca. 1.5% too high. Likely the effect of the impurity leads to less than 1% inaccuracy in the heat capacity. See Table I.

B. Thermodynamic stability of $HfMo_2O_8$

The temperature-dependent thermodynamics of the production of $HfMo_2O_8$(s) from HfO_2(s) and MoO_3(s) can now be quantified by the thermodynamic cycle shown in Fig. 2. The heat capacities are known for HfO_2(s) (Ref. 24) and for MoO_3(s) (Ref. 25). The enthalpies of formation at 298.15 K have been reported for HfO_2(s) and MoO_3(s), as -1145 kJ mol^{-1} and -745 kJ mol^{-1},[26,27] respectively. The enthalpy of formation for $HfMo_2O_8$(s) from HfO_2 and MoO_3 has been reported as 55.8 ± 3.1 kJ mol^{-1}.[28] With this information and the present heat capacity data, the enthalpy, entropy, and Gibbs energy changes for production of $HfMo_2O_8$(s) from HfO_2(s) and MoO_3(s) were determined as functions of temperature (Fig. 3). The Gibbs energy change for production of $HfMo_2O_8$(s) from its constituent oxides was found to be positive at room temperature, consistent with its metastable nature.[6] We now see (Fig. 3) that $(\partial\Delta_{prod}G/\partial T)_P$ is negative, so $HfMo_2O_8$ becomes less unstable at higher temperatures with respect to the oxides, in line with the known behavior of ZrW_2O_8.

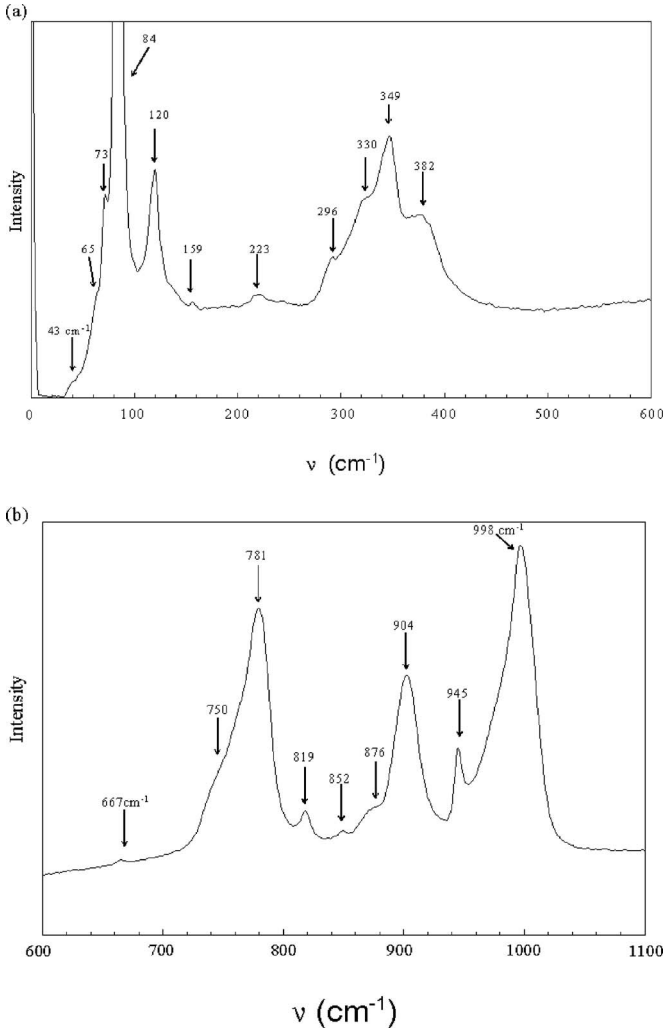

FIG. 5. Raman spectrum of $HfMo_2O_8$ at $T=300$ K with assigned peaks, (a) low-frequency region and (b) high-frequency region.

TABLE I. Experimental heat capacities for cubic $HfMo_2O_8$.

T (K)	C_P (J K^{-1} mol^{-1})	T (K)	C_P (J K^{-1} mol^{-1})	T (K)	C_P (J K^{-1} mol^{-1})
		PPMS ^{4}He, 10.781±0.010 mg			
2.061	0.0071±0.0005	12.06	4.23±0.02	63.68	66.4±0.4
2.283	0.0100±0.0001	13.38	5.45±0.02	70.66	74.6±0.3
2.535	0.0151±0.0005	14.85	6.91±0.03	78.40	83.1±0.4
2.811	0.0226±0.0016	16.48	8.64±0.07	86.99	92.2±0.3
3.121	0.0306±0.0035	18.29	10.7±0.0	96.52	101.7±0.7
3.462	0.0488±0.0166	20.29	13.0±0.1	107.10	111.9±0.6
3.846	0.0754±0.0022	22.51	15.8±0.2	118.84	121.7±0.6
4.264	0.120±0.002	24.98	18.9±0.1	131.85	131.6±0.4
4.731	0.174±0.007	27.71	22.3±0.1	146.30	141.4±0.5
5.248	0.275±0.014	30.75	26.2±0.2	162.35	150.9±0.2
5.822	0.416±0.010	34.12	30.4±0.1	180.14	160.1±0.2
6.474	0.638±0.004	37.86	35.3±0.1	199.86	168.7±0.4
7.173	0.900±0.009	42.01	40.4±0.2	221.72	177.4±0.5
7.956	1.28±0.00	46.62	46.2±0.2	245.97	185.5±0.5
8.828	1.77±0.01	51.72	52.4±0.2	272.82	194.2±1.3
9.794	2.42±0.01	57.39	59.3±0.1	302.67	198.7±1.3
10.87	3.23±0.01				
		PPMS ^{4}He, 14.002±0.010 mg			
2.035	0.0075±0.0003	11.48	3.72±0.05	64.22	67.1±0.5
2.221	0.0097±0.0002	12.52	4.64±0.02	70.01	73.7±0.5
2.425	0.0124±0.0009	13.64	5.68±0.07	76.29	80.3±0.3
2.648	0.0163±0.0013	14.85	6.93±0.05	83.17	87.7±0.6
2.888	0.0210±0.0010	16.18	8.33±0.10	90.65	95.3±0.9
3.154	0.0315±0.0030	17.64	9.93±0.04	98.83	103.5±0.1
3.443	0.0466±0.0011	19.22	11.7±0.1	107.73	111.7±0.3
3.758	0.0641±0.0055	20.96	13.8±0.2	117.44	119.8±0.4
4.099	0.0958±0.0028	22.84	16.1±0.4	128.01	127.9±0.3
4.466	0.140±0.006	24.88	18.6±0.2	139.53	136.0±0.3
4.865	0.205±0.010	27.12	21.6±0.2	152.09	143.8±0.6
5.309	0.279±0.014	29.57	24.7±0.1	165.81	151.3±0.2
5.785	0.411±0.004	32.22	28.1±0.1	180.76	158.9±0.2
6.300	0.579±0.016	35.12	31.7±0.2	197.01	165.7±0.2
6.886	0.759±0.250	38.29	35.8±0.1	214.73	173.0±0.2
7.453	1.02±0.01	41.74	40.0±0.1	234.00	178.4±0.5
8.128	1.37±0.00	45.50	44.7±0.1	255.04	185.3±0.4
8.858	1.80±0.01	49.59	49.7±0.1	277.93	191.4±0.8
9.658	2.32±0.01	54.06	55.0±0.1	303.02	200.0±1.0
10.53	2.96±0.01	58.92	60.7±0.1		
		PPMS ^{4}He, 10.230±0.010 mg			
3.980	0.0903±0.0009	5.549	0.349±0.002	8.280	1.47±0.01
4.254	0.119±0.001	5.929	0.451±0.002	8.850	1.81±0.02
4.546	0.155±0.002	6.340	0.575±0.009	9.440	2.18±0.01
4.858	0.204±0.001	6.775	0.738±0.004	10.02	2.54±0.02
5.194	0.268±0.001	7.240	0.935±0.004		
3.732	0.0691±0.0011	7.743	1.18±0.01		
		PPMS ^{4}He, 25.804±0.005 mg			
0.5330	$(2.07\pm0.14)\times10^{-4}$	1.398	$(2.50\pm0.11)\times10^{-3}$	105.52	109.0±1.4

TABLE I. (*Continued.*)

T (K)	C_P (J K^{-1} mol^{-1})	T (K)	C_P (J K^{-1} mol^{-1})	T (K)	C_P (J K^{-1} mol^{-1})
0.5667	$(2.52\pm0.14)\times10^{-4}$	1.498	$(3.20\pm0.08)\times10^{-3}$	116.10	117.8±1.4
0.6025	$(3.82\pm0.89)\times10^{-4}$	1.609	$(3.68\pm0.36)\times10^{-3}$	127.73	126.1±1.0
0.6962	$(4.08\pm0.06)\times10^{-4}$	1.726	$(4.57\pm0.18)\times10^{-3}$	140.53	134.7±1.5
0.7441	$(8.52\pm0.09)\times10^{-4}$	1.852	$(5.44\pm0.48)\times10^{-3}$		
0.7992	$(9.95\pm0.16)\times10^{-4}$	1.984	$(6.78\pm0.18)\times10^{-3}$		
0.8550	$(1.03\pm0.02)\times10^{-3}$	2.130	$(8.39\pm0.44)\times10^{-3}$		
0.9185	$(1.11\pm0.18)\times10^{-3}$	2.287	0.0103±0.0001		
0.9860	$(1.32\pm0.20)\times10^{-3}$	2.454	0.0129±0.0005		
1.056	$(1.50\pm0.06)\times10^{-3}$	2.636	0.0162±0.0004		
1.131	$(1.94\pm0.08)\times10^{-3}$	2.830	0.0208±0.0002		
1.215	$(2.01\pm0.19)\times10^{-3}$	3.035	0.0273±0.0002		
1.302	$(2.29\pm0.18)\times10^{-3}$	95.91	100.5±1.0		

C. Lattice dynamical contributions to the heat capacity

Of the 132 degrees of freedom associated with the unit cell of $HfMo_2O_8$, 3 are acoustic modes and 129 are optic modes. The acoustic modes can be quantified from the Debye temperature θ_D determined from the Debye-T^3 law

$$C_V = \frac{12}{5}\pi^4 N_A k_B \left(\frac{T}{\theta_D}\right)^3, \quad (1)$$

using heat capacity data in the low-T range 0.4–2.6 K and assuming $C_V = C_P$ at these low temperatures. The slope of C_P vs T^3 for $HfMo_2O_8$ at limiting low temperatures (Fig. 4) gives a value of $\theta_D = 82$ K for 3 degrees of freedom in the unit cell containing 4 formula units—i.e., assuming that the optic modes contribute negligibly for $T < 2.6$ K. This value of θ_D is similar to but slightly less than the value obtained for ZrW_2O_8 using the same methods, $\theta_D = 88$ K.[20]

The optic modes for $HfMo_2O_8$ have not been assessed previously. From the present determination of its Raman spectrum (Fig. 5), 20 frequencies were distinguished. By analogy with ZrW_2O_8,[29] we expect an additional mode below our lowest measurable frequency, at about 28 cm^{-1}. In parallel with the assignment of optic modes for ZrW_2O_8,[20,30,31] we present the optic mode assignment in Table II.

The contributions to C_V for $HfMo_2O_8$ are shown in Fig. 6 in comparison with the experimental values of C_V [derived from measured values of C_P using the known thermal expansion coefficient (Ref. 4) and the bulk modulus of $ZrMo_2O_8$ (Ref. 6)]. Except for the highest and lowest temperatures,

TABLE II. Observed Raman frequencies for $HfMo_2O_8$ and assigned degeneracies for the calculation of the optic mode contribution to the heat capacity.

T=298 K			T=298 K		
(cm^{-1})	(meV)	Degeneracy	(cm^{-1})	(meV)	Degeneracy
(29)[a]	(3.5)[a]	1	667	82.7	3.556
43	5.3	1	750	93.0	3.556
65	8.1	2	781	96.8	3.556
74	9.1	9	819	101.5	3.556
84	10.4	9	852	105.6	3.556
120	14.9	9	876	108.6	3.556
159	19.7	9	904	112.1	3.556
223	22.6	9	945	117.2	3.556
296	36.7	13	998	123.7	3.556
330	40.9	13			
349	43.3	11			
382	47.4	11			
	Subtotal	97		Subtotal	32
		Total: 129			

[a]By analogy with results from the IR study of ZrW_2O_8 (Ref. 29).

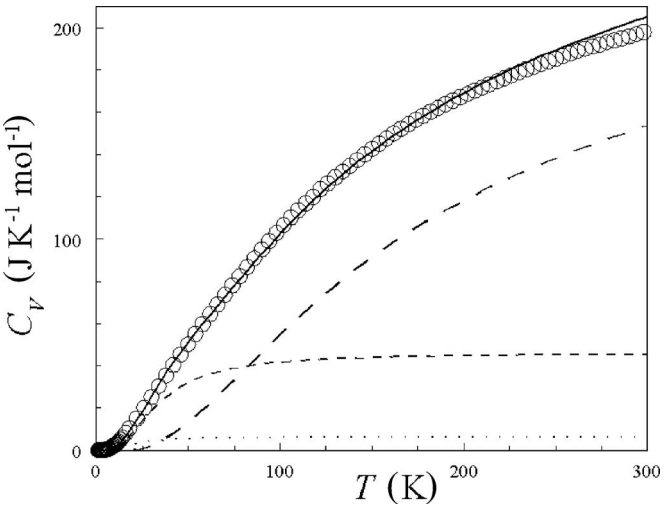

FIG. 6. Heat capacity of $HfMo_2O_8$. ○ experimental data, (solid line) total calculated, (short-dashed line) optic with energies <10 meV, (dashed line) optic with energies >10 meV, and (dotted line) acoustic.

which show deviations up to 5% for $T>250$ K and >10% for $T<20$ K, the calculated and experimental values of C_V are in excellent agreement. Since optic modes dominate, this shows that the general assignment, and particularly the abundance of low-frequency optic modes and the gap between about 400 cm^{-1} and 700 cm^{-1}, as for other AB_2O_8 NTE materials,[32] accurately represents the lattice dynamics of $HfMo_2O_8$.

D. Comparison of $HfMo_2O_8$ with other AB_2O_8 compounds

The heat capacity of $HfMo_2O_8$ is quantitatively very similar to that of α-ZrW_2O_8 (Fig. 7) although the two structures are slightly different. ($HfMo_2O_8$ has the same structure as the high-temperature phase of ZrW_2O_8 in which the $[WO_4]^{2-}$ tetrahedra are disordered randomly either in the [111] or

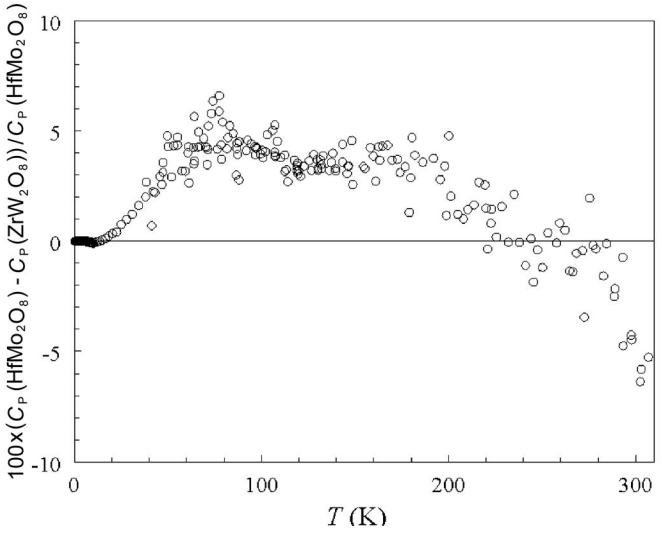

FIG. 7. Relative heat capacity differences between $HfMo_2O_8$ and ZrW_2O_8.

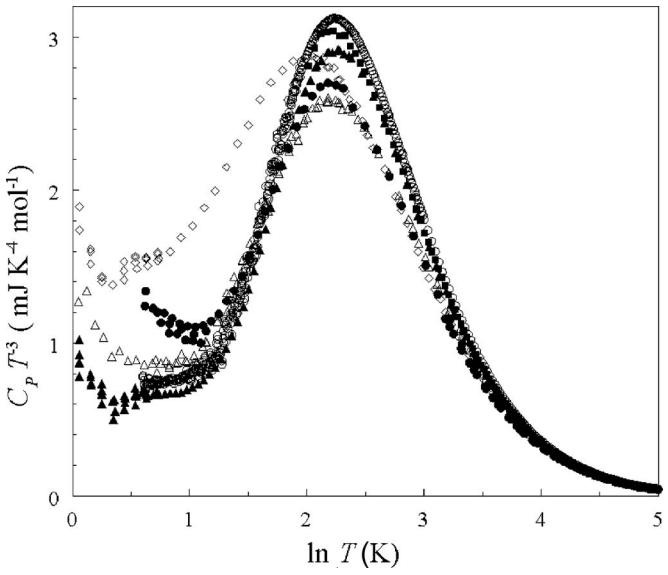

FIG. 8. C_PT^{-3} vs ln(T) for AB_2O_8 NTE materials. α-ZrW_2O_8: ● Kennedy and White (Ref. 22), ■ Yamamura *et al.* (Ref. 17 and 19), and ▲ Stevens *et al.* (Ref. 18). Cubic-HfW_2O_8: ○ Yamamura *et al.* (Ref. 17); cubic-$ZrMo_2O_8$: ◇ Stevens *et al.* (Ref. 18); cubic-$HfMo_2O_8$: △ present study.

$[\bar{1}\bar{1}\bar{1}]$ direction in a 1:1 ratio.[33]) We find (Fig. 7) that the heat capacity of $HfMo_2O_8$ exceeds that of ZrW_2O_8 at low temperatures, but the trend reverses above about 240 K. The maximum value of the absolute heat capacity difference is ~5 J K^{-1} mol^{-1} at approximately $T=100$ K. (If the reported heat capacities were 1% too high due to amorphous $HfMo_2O_8$, the zero line in Fig. 7 would shift up by 1%.) On the basis of the *effective* Debye temperature θ_D^e—i.e., treating all the lattice modes (3 acoustic and 129 optical) as Debye-like—Yamamura *et al.*[34] showed that bonds in HfW_2O_8 are, on average, 1.15 times stiffer than in ZrW_2O_8. Similar analysis here indicates that the bonds in $HfMo_2O_8$ have, on average, about the same stiffness as in ZrW_2O_8. Although the HfW_2O_8/ZrW_2O_8 stiffness ratio scaled well with the reciprocal of the molecular masses,[34] the $HfMo_2O_8/ZrW_2O_8$ comparison does not, indicating that the overall lattice dynamics are not determined by mass alone.

Cao *et al.* proposed mechanisms for NTE in ZrW_2O_8 that stressed the importance of vibrations of the polyhedra.[35,36] The $[WO_4]^{2-}$ units are rigid, whereas $[ZrO_6]^{8-}$ octahedra are stiff but not rigid, and the low-energy vibrations of the undistorted polyhedra strongly depend on the type of cation at the center of the polyhedron.[34] Consequently, the mass change could be expected to affect the thermal expansion coefficient; $HfMo_2O_8$ has a slightly smaller absolute thermal expansion coefficient than β-ZrW_2O_8: $\alpha_l(HfMo_2O_8)$ is -4.0×10^{-6} K^{-1} for $T=77-573$ K (Ref. 4) compared with $\alpha_l(\beta\text{-}ZrW_2O_8)$ of -6.2×10^{-6} K^{-1} for $T=500-560$ K (Ref. 37).

A study by Yamamura *et al.* compared α-HfW_2O_8 to isostructural α-ZrW_2O_8, (Ref. 34) in terms of C_P and thermal expansion values. Despite the large difference in atomic masses of Hf and Zr, their thermal expansion coefficients are very similar: $\alpha_l(HfW_2O_8)$ is -8.8×10^{-6} K^{-1} and

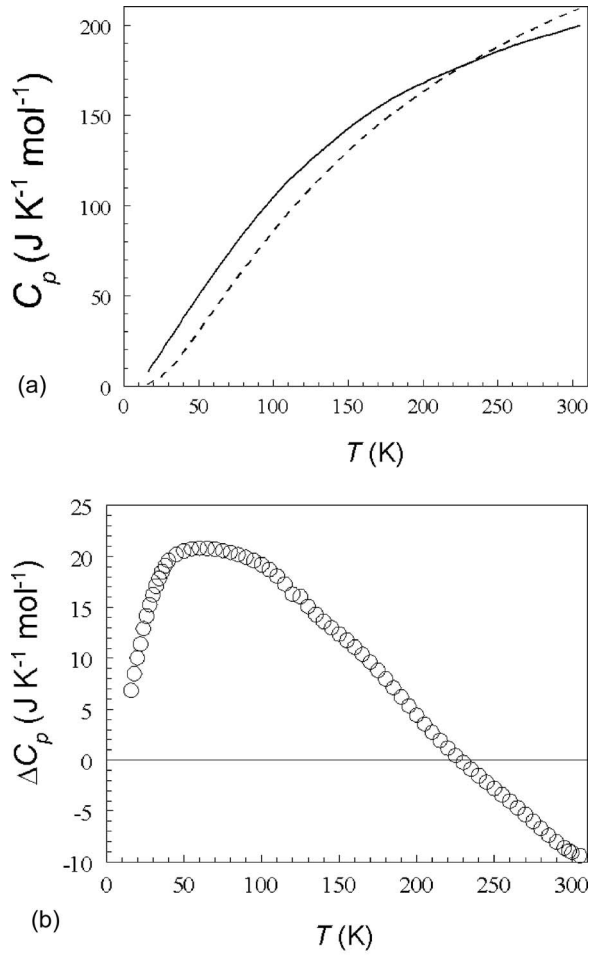

FIG. 9. Heat capacity of hafnium molybdate relative to the sum of its binary oxides. (a) solid line: experimental C_P of $HfMo_2O_8$; dashed line: constituent additivity of binary oxides—i.e., $C_P(HfO_2)+2\times C_P(MoO_3)$; (b) $\Delta C_P=C_P(HfMo_2O_8)-C_P(HfO_2)-2C_P(MoO_3)$.

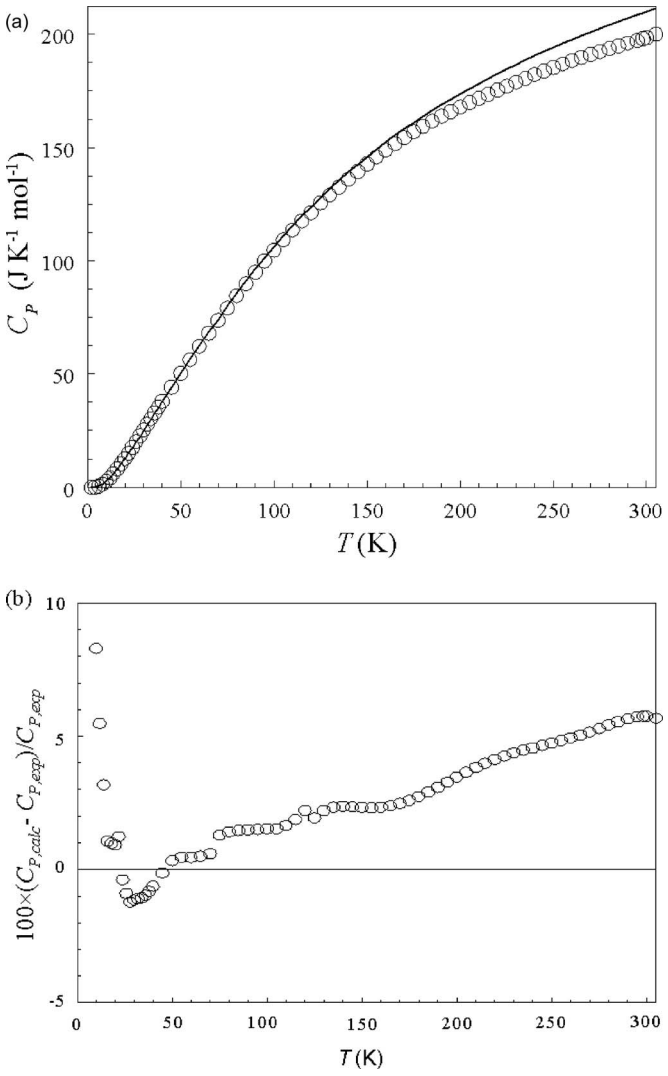

FIG. 10. (a) Heat capacity of hafnium molybdate from the sum of its AB_2O_8 oxides, solid line: $C_P(HfW_2O_8)-C_P(ZrW_2O_8)+C_P(ZrMo_2O_8)$ and ○ smoothed experimental $C_P(HfMo_2O_8)$. (b) Relative deviation of calculated C_P from measured C_P.

$\alpha_l(\alpha\text{-}ZrW_2O_8)$ is -9.6×10^{-6} K^{-1} (both for $T=90-300$ K).[37] The heat capacities also are quantitatively similar: the values of $\Delta C_P=C_P(HfW_2O_8)-C_P(ZrW_2O_8)$ are maximal at approximately 3 J K^{-1} mol^{-1} at $T=80$ K and ΔC_P goes from positive to negative above $T\sim200$ K.[34]

Stevens *et al.*[18] compared the heat capacities of α-ZrW_2O_8 and cubic-$ZrMo_2O_8$ (which is isostructural with β-ZrW_2O_8) and found their C_P values to be very similar, within about 4 J K^{-1} mol^{-1} with ZrW_2O_8 higher at lower temperatures, crossing over at about $T=180$ K. Their thermal expansion coefficients are very similar: $\alpha_l(ZrMo_2O_8)=-5.0\times10^{-6}$ K^{-1} for $T<600$ K (Ref. 6) and $\alpha_l(\beta\text{-}ZrW_2O_8)=-6.2\times10^{-6}$ K^{-1} for $T=500-560$ K. (Ref. 37).

The low-frequency lattice dynamics can be assessed through a plot of C_PT^{-3} vs $\ln(T)$, as given in Fig. 8 for all the AB_2O_8 NTE materials for which the C_P values have been reported. The bell-shaped curves are similar for all AB_2O_8 compounds and are centered at approximately $T=9.5$ K, except for $ZrMo_2O_8$, which is centered at approximately $T=8$ K. The difference in peak location and shape suggests that the distribution of low-frequency optic modes is similar for α-ZrW_2O_8, cubic-HfW_2O_8, and cubic-$HfMo_2O_8$, but slightly different in $ZrMo_2O_8$.

E. Constituent additivity

The Neumann-Kopp law is based on the additivity of the heat capacity properties of the constituent atoms as an estimate of the heat capacity of a solid. It can be used to describe simple solids such as binary compounds and alloys.[38] A similar approach concerned with the thermodynamic contribution from the "constituent group" of a compound has been used with considerable success to estimate the heat capacity and thermodynamics of complex inorganic compounds.[39–41] For example, the constituent additivity method has been used to estimate the heat capacity of sodalite $Na_8Al_6Si_6O_{24}Cl_2$ to within a few percent for 100 K$<T<$1000 K.[41]

Stevens *et al.* have used this technique to calculate C_P of α-ZrW_2O_8 and cubic-$ZrMo_2O_8$ from the weighted sums of their constituent binary oxides.[18] They found for both com-

pounds that the C_P from the sum of the binary oxides was smaller than the experimental C_P. $\Delta C_P = C_P(AB_2O_8) - C_P(AO_2) - 2C_P(BO_3)$ was at the maximum ~ 27 J K^{-1} mol^{-1} for α-ZrW_2O_8 and was at the maximum ~ 23 J K^{-1} mol^{-1} for cubic-$ZrMo_2O_8$. The maximum for ΔC_P for both NTE materials occurred at approximately $T = 80$ K. This led them to infer that there exist a significant number of low-energy vibrational modes in the NTE materials relative to the binary oxides.

Similar analysis for another NTE oxide, Zn_2GeO_4, showed[42] an excess C_P relative to hexagonal ZnO and tetragonal GeO_2 with a maximum value of ~ 12 J K^{-1} mol^{-1} at approximately $T = 100$ K, again due to low-frequency modes that do not exist in the binary oxides. There is a correlation between the lower magnitude of the coefficient of thermal expansion for Zn_2GeO_4 than ZrW_2O_8 and $ZrMo_2O_8$ and the lower magnitude of the excess C_P (decreasing excess C_P with thermal expansion magnitude).

The heat capacities of $HfMo_2O_8$ were compared with the sum of the C_P values of its constituent binary oxides HfO_2 and MoO_3 (Fig. 9). $C_P(HfO_2)$ for $52\ \mathrm{K} < T < 300$ K is from Todd;[24] experimental data for $T < 50$ K appear not to have been published, however, Todd's data were extrapolated to lower temperatures by Westrum *et al.*[43] The heat capacities of MoO_3 have recently been measured.[25] Figure 9(b) shows that for $T < 200$ K, there is a large excess in C_P of $HfMo_2O_8$ (as much as ~ 20 J K^{-1} mol^{-1} at about 50 K) relative to the sum of its binary oxides. We conclude that there exist a significant number of low-energy vibrational modes in $HfMo_2O_8$ relative to the binary oxides, as was seen for $ZrMo_2O_8$ and ZrW_2O_8 (Ref. 18) and, to a lesser extent, Zn_2GeO_4 (Ref. 42).

We can compare the $C_P(HfMo_2O_8)$ data with a calculation of $C_P(HfMo_2O_8)$ from the other oxides—i.e., $C_{P,exp}(HfMo_2O_8)$ vs $C_{P,calc}(HfMo_2O_8) = C_P(HfW_2O_8) - C_P(ZrW_2O_8) + C_P(ZrMo_2O_8)$. [The values of $C_P(HfW_2O_8)$, published only in figure form by Yamamura *et al.*,[17] were obtained from the authors.] Use of the heat capacities of the NTE AB_2O_8 materials provides a better fit (Fig. 10) than using the binary oxides (Fig. 9). (If the reported heat capacities were 1% too high due to amorphous $HfMo_2O_8$, the zero line in Fig. 10 would shift down by 1%.) This is reasonable since the AB_2O_8 materials all exhibit NTE and therefore would have the low-frequency optic modes (which give rise to NTE) that the binary oxides do not have.

IV. CONCLUDING REMARKS

The present thermodynamic analysis shows that $HfMo_2O_8$ is metastable with respect to HfO_2 and MoO_3 at ambient temperature. From the lattice dynamic perspective, $HfMo_2O_8$ is very similar to other AB_2O_8 materials that exhibit negative thermal expansion, with a dominance of low-frequency optical modes. The heat capacity of $HfMo_2O_8$ is markedly different from the sum of its constituent oxides HfO_2 and MoO_3, which do not exhibit NTE.

ACKNOWLEDGMENTS

The authors gratefully acknowledge financial support from NSERC, the Killam Trusts, the Canada Foundation for Innovation, Atlantic Innovation Fund, and other partners that fund the Facilities for Materials Characterization managed by the Institute for Research in Materials. We are grateful to M. Jakubinek and M. Stancescu for experimental assistance and C. Lind for helpful discussions. The work performed at the Georgia Institute of Technology was supported by the U.S. NSF through Grant Nos. DMR-0203342 and DMR-0605671.

*Corresponding author. FAX: 1 (902) 494-8016. Electronic address: Mary.Anne.White@dal.ca

[1] C. Martinek and F. A. Hummel, J. Am. Ceram. Soc. **51**, 227 (1968).
[2] J. S. O. Evans, T. A. Mary, T. Vogt, M. A. Subramanian, and A. W. Sleight, Chem. Mater. **8**, 2809 (1996).
[3] T. A. Mary, J. S. O. Evans, T. Vogt, and A. W. Sleight, Science **272**, 90 (1996).
[4] C. Lind, Ph.D. thesis, Georgia Institute of Technology, 2001.
[5] S. N. Achary, G. D. Mukherjee, A. K. Tyagi, and B. K. Godwal, Phys. Rev. B **66**, 184106 (2002).
[6] C. Lind, A. P. Wilkinson, Z. Hu, S. Short, and J. D. Jorgensen, Chem. Mater. **10**, 2335 (1998).
[7] M. Auray, M. Quarton, and P. Tarte, Powder Diffr. **2**, 36 (1987).
[8] C. Lind, D. G. VanDerveer, A. P. Wilkinson, J. Chen, M. T. Vaughan, and D. J. Weidner, Chem. Mater. **13**, 487 (2001).
[9] S. N. Achary, G. D. Mukherjee, A. K. Tyagi, and B. K. Godwal, Powder Diffr. **18**, 147 (2003).
[10] S. R. Bharadwaj, M. S. Samant, R. Mishra, S. R. Dharwadkar, S. S. Savant, and R. Kalyanaraman, J. Alloys Compd. **230**, 13 (1995).
[11] R. Pankajavalli and O. M. Sreedharan, J. Nucl. Mater. **175**, 194 (1990).
[12] Z. Singh, S. Dash, R. Prasad, and V. Venugopal, J. Alloys Compd. **244**, 85 (1996).
[13] M. S. Samant, S. R. Bharadwaj, A. S. Kerkar, and S. R. Dharwadkar, J. Nucl. Mater. **207**, 98 (1993).
[14] J. S. Hwang, K. J. Lin, and C. Tien, Rev. Sci. Instrum. **68**, 94 (1997).
[15] C. A. Kennedy, M. Stancescu, R. A. Marriott, and M. A. White, Cryogenics **47**, 107 (2007).
[16] A. P. Ramirez and G. R. Kowach, Phys. Rev. Lett. **80**, 4903 (1998).
[17] Y. Yamamura, N. Nakajima, T. Tsuji, Y. Iwasa, K. Saito, and M. Sorai, Solid State Commun. **121**, 213 (2002).
[18] R. Stevens, J. Linford, B. F. Woodfield, J. Boerio-Goates, C. Lind, A. P. Wilkinson, and G. Kowach, J. Chem. Thermodyn. **35**, 919 (2003).
[19] Y. Yamamura, T. Tsuji, K. Saito, and M. Sorai, J. Chem. Thermodyn. **36**, 525 (2004).
[20] C. A. Kennedy, Ph.D. thesis, Dalhousie University, 2005.
[21] C. A. Kennedy, M. A. White, A. P. Wilkinson, and T. Varga, Appl.

Phys. Lett. **90**, 151906 (2007).
[22] C. A. Kennedy and M. A. White, Solid State Commun. **134**, 271 (2005).
[23] *PPMS Hardware and Options Manual*, 2nd ed. (Quantum Design, San Diego, 1999).
[24] S. S. Todd, J. Am. Chem. Soc. **75**, 3035 (1953).
[25] J. Boerio-Goates (private communication).
[26] E. J. Huber, Jr. and C. E. Holley, Jr., J. Chem. Eng. Data **13**, 252 (1968).
[27] M. W. Chase, Jr., J. Phys. Chem. Ref. Data Monogr. **9**, 1 (1998).
[28] T. Varga, C. Lind, A. P. Wilkinson, H. Xu, C. E. Lesher, and A. Navrotsky, Chem. Mater. **19**, 468 (2007).
[29] J. N. Hancock, C. Turpen, Z. Schlesinger, G. R. Kowach, and A. P. Ramirez, Phys. Rev. Lett. **93**, 225501 (2004).
[30] G. Ernst, C. Broholm, G. R. Kowach, and A. P. Ramirez, Nature (London) **396**, 147 (1998).
[31] T. R. Ravindran, A. K. Arora, and T. A. Mary, J. Phys.: Condens. Matter **13**, 11573 (2001).
[32] R. Mittal, S. L. Chaplot, and N. Choudhury, Prog. Mater. Sci. **51**, 211 (2006).
[33] Y. Yamamura, N. Nakajima, and T. Tsuji, Solid State Commun. **114**, 453 (2000).
[34] Y. Yamamura, N. Nakajima, T. Tsuji, M. Koyano, Y. Iwasa, S. Katayama, K. Saito, and M. Sorai, Phys. Rev. B **66**, 014301 (2002).
[35] D. Cao, F. Bridges, G. R. Kowach, and A. P. Ramirez, Phys. Rev. Lett. **89**, 215902 (2002).
[36] D. Cao, F. Bridges, G. R. Kowach, and A. P. Ramirez, Phys. Rev. B **68**, 014303 (2003).
[37] Y. Yamamura, N. Nakajima, and T. Tsuji, Phys. Rev. B **64**, 184109 (2001).
[38] E. S. R. Gopal, *Specific Heats at Low Temperatures* (Plenum Press, New York, 1966).
[39] B. J. Wood, in *Thermodynamics of Minerals and Melts*, Advances in Physical Geochemistry, Vol. 1, edited by R. C. Newton, A. Navrotsky, and B. J. Wood (Springer-Verlag, New York, 1981).
[40] B. F. Woodfield, J. Boerio-Goates, J. L. Shapiro, R. L. Putnam, and A. Navrotsky, J. Chem. Thermodyn. **31**, 245 (1999).
[41] L. Qiu and M. A. White, J. Chem. Educ. **78**, 1076 (2001).
[42] R. Stevens, B. F. Woodfield, J. Boerio-Goates, and M. Crawford, J. Chem. Thermodyn. **36**, 349 (2004).
[43] E. F. Westrum, Jr., B. H. Justice, J. A. Sommers, and D. A. Johnson, J. Therm Anal. Calorim. **57**, 659 (1999).